Research paper

Tropolone-induced effects on the unfolded protein response pathway and apoptosis in multiple myeloma cells are dependent on iron

Staci L. Haney[a], Michelle L. Varney[a], Hannah R. Safranek[a], Yashpal S. Chhonker[b], Narendran G-Dayanandan[c], Geoffrey Talmon[d], Daryl J. Murry[b], Andrew J. Wiemer[c], Dennis L. Wright[c], Sarah A. Holstein[a],[*]

[a] Department of Internal Medicine, University of Nebraska Medical Center, Omaha, NE, United States
[b] Department of Pharmacy Practice, University of Nebraska Medical Center, Omaha, NE, United States
[c] Department of Pharmaceutical Sciences, University of Connecticut, Storrs, CT, United States
[d] Department of Pathology and Microbiology, University of Nebraska Medical Center, Omaha, NE, United States

A B S T R A C T

Tropolones are naturally occurring seven-membered non-benzenoid aromatic compounds that are of interest due to their cytotoxic properties. MO-OH-Nap is a novel α-substituted tropolone that induces caspase cleavage and upregulates markers associated with the unfolded protein response (UPR) in multiple myeloma (MM) cells. Given previous reports that tropolones may function as iron chelators, we investigated the effects of MO-OH-Nap, as well as the known iron chelator deferoxamine (DFO), in MM cells in the presence or absence of supplemental iron. The ability of MO-OH-Nap to induce apoptosis and upregulate markers of the UPR could be completely prevented by co-incubation with either ferric chloride or ammonium ferrous sulfate. Iron also completely prevented the decrease in BrdU incorporation induced by either DFO or MO-OH-Nap. Ferrozine assays demonstrated that MO-OH-Nap directly chelates iron. Furthermore, MO-OH-Nap upregulates cell surface expression and mRNA levels of transferrin receptor. In vivo studies demonstrate increased Prussian blue staining in hepatosplenic macrophages in MO-OH-Nap-treated mice. These studies demonstrate that MO-OH-Nap-induced cytotoxic effects in MM cells are dependent on the tropolone's ability to alter cellular iron availability and establish new connections between iron homeostasis and the UPR in MM.

1. Introduction

Tropolones are small, naturally occurring organic compounds that make ideal scaffolds for drug development. Several tropolone derivatives have anti-proliferative effects in a variety of cancer cell lines, which has led to investigation into the use of tropolones as anti-cancer agents [1–4]. Beta-thujaplicin, a naturally occurring and well-studied tropolone, has anti-cancer activity in a variety of mouse tumor models, including melanoma, breast, and lung cancer [5–7]. Tropolones have been shown to inhibit select metalloenzymes, including histone deacetylase (HDAC) 2 and 8, and may have activity as iron-chelating agents. [8–13].

Multiple myeloma (MM) is a bone marrow malignancy characterized by the abnormal proliferation of clonal plasma cells which produce monoclonal protein. It is predicted that in 2018 over 30,000 individuals will be diagnosed with MM and over 12,000 will die from MM in the United States. [14] While new treatment options have prolonged patient survival, the majority of patients will eventually die of relapsed/refractory MM. Thus there continues to be a need for novel treatment strategies. Recently, our group examined the activity of six novel α-substituted tropolones, including MO-OH-Nap (2-hydroxy-7-naphthalene-2-yl-cyclohepta-2,4,6-trienone), in MM cells and demonstrated that MO-OH-Nap induces caspase cleavage in a time frame distinct from that of the pan-HDAC inhibitor suberoylanilide hydroxamic acid (SAHA) [15]. MO-OH-Nap, but not SAHA, promotes the expression of markers associated with endoplasmic reticulum (ER)

stress and the unfolded protein response (UPR) in MM cells. MO-OH-Nap also displayed synergistic effects when used in conjunction with the proteasome inhibitor bortezomib but in a manner that was independent of aggresome formation [15]. These findings prompted further investigation into MO-OH-Nap's mechanism of action in MM.

Previous studies in leukemia cell lines demonstrated that co-incubation with Fe^{3+} mitigates the anti-proliferative effects of various tropolones, including MO-OH-Nap [2]. However, whether the ability of MO-OH-Nap to induce the UPR is dependent on the agent's activity as an iron chelator is unknown. We therefore evaluated the iron-dependency of MO-OH-Nap as well as the effects of the known iron chelator deferoxamine (DFO) in MM cells. We found that DFO upregulates markers of the UPR and that co-incubation with either ferric chloride (FC) or ammonium ferrous sulfate (AFS) prevents the MO-OH-Nap-induced increase in apoptosis and UPR activation. Collectively, these studies reveal that the ability of MO-OH-Nap to induce the UPR and apoptosis in MM cells is iron-dependent.

2. Material and methods

2.1. Reagents and cell culture

MO-OH-Nap was synthesized as previously described [2,10]. Stock solutions of MO-OH-Nap were prepared in DMSO (10 mM) and stored at −20 °C. Suberoylanilide hydroxamic acid (SAHA), bortezomib, DFO, FC, AFS and zinc chloride were purchased from Sigma-Aldrich (St Louis, MO, USA).

2.2. Cell culture

RPMI-8226, MM.1S, and U266 cell lines were purchased from American Type Culture Collection (ATCC) (Manassas, VA, USA). Cells were grown in media supplemented with heat-inactivated fetal bovine serum, glutamine and penicillin-streptomycin at 37 °C and 5% CO_2.

2.3. Immunoblotting

Cells were incubated in the presence of drugs with or without iron for either 24 or 48 h, washed with PBS, and lysed in RIPA buffer supplemented with protease and phosphatase inhibitors (0.15 M NaCl, 1% sodium deoxycholate, 0.1% SDS, 1% (v/v) Triton X-100, 0.05 M Tris HCl, pH 7.4). Protein quantification was determined using the BCA method. Equal amounts of total protein were run on SDS-PAGE gels, transferred to polyvinylidene difluoride membranes, and probed with applicable primary and secondary antibodies (Supplemental Table 1). Proteins were visualized using an ECL chemiluminescence detection kit and a Bio-Rad ChemiDoc MP imaging system.

2.4. Apoptosis assay

U266 cells were treated with solvent control (DMSO), MO-OH-Nap or DFO for 48 h with or without the addition of iron. Cells were washed and stained with APC-conjugated Annexin V antibody and propidium iodide (PI) according to the manufacturer's recommendations (eBioscience, San Diego, CA, USA). From each tube, 10,000 cells were analyzed using a BD LSRII flow cytometer. Data analysis and flow diagrams were accomplished using FlowJo software. Early apoptotic cells are defined as those positive for Annexin V and negative for PI while late apoptotic/necrotic cells are those positive for both markers [16].

2.5. BrdU incorporation assay

MM cells were grown in 96-well tissue culture plates at 2.5×10^4 cells/100 μL/well (RPMI-8226) or 5×10^4 cells/100 μL/well (U266). Cells were incubated for 48 h with solvent control (DMSO) or varying concentrations of drugs and/or iron. BrdU was added four (RPMI-8226) or six (U266) hours prior to fixation. Plates were spun at 1000 rpm for 10 min. Cell processing occurred per manufacturer's instructions using the Millipore BrdU Cell Proliferation Assay kit.

2.6. Ferrozine iron chelation assay

All reactions were performed in triplicate in a 96-well microplate. 100 μL of DFO or MO-OH-Nap solutions (dissolved in DMSO) were mixed with AFS (50 μL, final concentration of 0.25 mM, dissolved in H_2O) and incubated at room temperature for 5 min. Ferrozine (50 μL dissolved in DMSO, final concentration of 1 mM and purchased from Sigma-Aldrich (St Louis, MO, USA)) was then added to the iron-chelator mixture. After 5 min, absorbance at 540 nm was recorded. Readings were normalized to the ferrozine-only control (50 μL ferrozine, 100 μL DMSO, and 50 μL AFS) using the following calculation: % Iron chelation = [(Absorbance control-Absorbance sample)/Absorbance control]*100.

2.7. qRT-PCR analysis

Cells were incubated for 24 h in the presence of DMSO or drug. 50 μM AFS was added concurrently with drug. RNA was isolated using the E.Z.N.A. HP total RNA kit from Omega Bio-tek (Norcross, VA, USA). 1 μg of total RNA was reverse transcribed to cDNA using the i-Script cDNA synthesis kit (Bio-Rad, Hercules, CA, USA). cDNA, gene specific primers, and i-Taq Sybr green super mix (Bio-Rad) were mixed according to manufacturer's instruction. qRT-PCR reactions were performed in duplicate in a CFX96 real time machine (Bio-Rad), and data was analyzed using the Bio-Rad CFX manager 3.1 software. Expression values were normalized to the house-keeping gene β-actin.

2.8. Cell cycle analysis

Cells were incubated for 48 h in the presence of solvent control (DMSO) or drug with or without iron. Next, to label and fix cells for flow cytometry, we re-suspended in 0.5 mL of cold hypotonic PI solution (50 μg/ml PI and 0.1% sodium citrate solution dissolved in water). Cells were vortexed and stored on ice for at least 15 min prior to data acquisition. From each tube, 20,000 cells were analyzed using a BD LSRII flow cytometer. Data analysis and flow diagrams were accomplished using FlowJo software.

2.9. Detection of reactive oxygen species (ROS)

Cells were plated at a density of 0.5×10^6 cells per well into six-well plates in complete culture medium containing 10 μM of chloromethyl 2′, 7′-dichlorodihydrofluorescein diacetate (CM-H_2DCFDA, Thermo Fisher, Waltham, MA, USA) and appropriate drug or solvent control (DMSO). FC (50 μM) was added concurrently with drug. 24 or 48 h later, the cells were washed and re-suspended in PBS. Positive controls were incubated with hydrogen peroxide (100 μM) for 1 h. Cells were incubated with PI (1 mg/mL) for at least 15 min prior to data analysis. Living cells, which are PI-negative, were selected by FACS gating. In these living cells, the fluorescence of CM-H2DCFDA was recorded. Data was obtained using a BD LSRII flow cytometer and analyzed with FlowJo software.

2.10. Animal studies and histology

Female 6–8 week-old CD-1 mice were purchased from Charles River and housed in the University of Nebraska Medical Center (UNMC) animal facility at a temperature of 23–25 °C, relative humidity of 50–70% and 12/12 h light/dark cycles. CD-1 mice are an outbred strain that are routinely used in toxicology studies. All studies were carried out in accordance with the Guide for the Care and Use of Laboratory Animals

(U.S. National Institutes of Health) and were approved by the UNMC IACUC (protocol number 17-014-04-FC). MO-OH-Nap was dissolved in a 5% DMSO, 45% W/V hydroxypropyl- β-cyclodextrin solution in PBS (final concentration 1.3 mg/mL MO-OH-Nap). The solution was filter sterilized and stored at $-20\,°C$. Standard dose escalation procedures were followed using the up-and-down method. To conserve animals, one mouse was injected at a time via tail vein. Dose escalation continued until the dose of 9.4 mg/kg was reached which represented the limit of solubility of the drug. At that point, multi-dose testing began such that mice were injected with 9.4 mg/kg MO-OH-Nap via the tail vein three times per week for a total of four weeks. Blood samples were analyzed using an Abaxis Vetscan2 instrument and the Preventative Care Profile Plus rotor. Complete blood count (CBC) measurements were obtained via whole blood using a scil Vet ABC Instrument. Tissues were fixed with formalin, imbedded, sectioned, and stained with Prussian blue dye or H&E using standard procedures in the UNMC Tissue Sciences Facility.

2.11. In vitro metabolism studies

Mouse S9 stability experiments were conducted utilizing a solution containing Tris buffer (50 mM, pH 7.4), mouse S9 fraction (1 mg/mL, XenoTech, LLC, Lenexa, KS, USA), magnesium chloride (20 mM), NADPH (2 mM), uridine diphosphate glucuronyltransferase (Sigma-Aldrich, MO) (2 mM), Adenosine 3′-Phosphate 5′-Phosphosulfate (PAPS, Sigma-Aldrich, MO) (0.1 mM) and saccharolactone (Sigma-Aldrich, MO) (5 mM). The reaction mixture (final volume 1.0 mL) was pre-incubated at 37 °C for 10 min in a water bath maintaining 60 rpm. The reaction was initiated upon addition of 2 μM final concentration of MO-OH-Nap (2 μL from 1 mM stock). Samples (100 μL) were collected at different time intervals (0, 5, 10, 20, 30, 45 60 and 90 min) and quenched with 300 μL of methanol: acetonitrile (1:1). Testosterone, 7-HC and diclofenac were used as positive controls. Supernatants (10 μL) were then analyzed by LC–MS/MS. The S9 fraction is a supernatant obtained from mouse liver homogenate by centrifuging at 9000 g.

2.12. Statistics

Two-tailed *t*-testing was used to calculate statistical significance. An α of 0.05 was set as the level of significance. Combination indices for the BrdU assays were determined via CalcuSyn software (Biosoft) which analyzes drug interactions based on the method of Chou and Talalay [17].

3. Results

3.1. Iron reverses the cytotoxic effects of MO-OH-Nap

As shown in Fig. 1a, incubation with MO-OH-Nap or DFO for 48 h induces the expression of proteins associated with apoptosis, including PARP and cleaved caspases 3, 8, and 9 in MM cell lines. Importantly, co-incubation with exogenous ferric or ferrous iron at a concentration of 50 μM completely prevents the induction of apoptotic markers in MO-OH-Nap- and DFO-treated cells. Furthermore, the addition of iron 24 h after the start of MO-OH-Nap incubation partially prevents the induction of apoptotic markers (Fig. 1b). In U266 cells, as little as 5 μM FC or AFS is sufficient to block induction of apoptotic markers (PARP, cleaved caspases 3, 8, and 9) and a UPR marker (phosphorylated-eIF2α (p-eIF2α)) (Fig. 1c). Likewise, Annexin V/PI flow cytometric studies demonstrate that iron prevents the MO-OH-Nap- and DFO-induced increase in early apoptotic and late apoptotic/necrotic cells in a concentration-dependent manner (Fig. 1d and Supplemental Fig. 1). Iron also inhibited MO-OH-Nap-induced apoptosis at 24- and 72-hour timepoints (Supplemental Fig. 2). BrdU incorporation experiments revealed that iron blocks the inhibition in cellular proliferation caused by MO-OH-Nap and DFO (Fig. 1e-f). Co-incubation with zinc does not prevent

either MO-OH-Nap or DFO-induced cytotoxic effects (Supplemental Fig. 3). Because tropolones are postulated to function as HDAC inhibitors and MO-OH-Nap can induce changes in histone acetylation [2,15], we examined the effect of iron on the activity of the pan-HDAC inhibitor, SAHA. Co-incubation with either FC or AFS did not alter SAHA-induced inhibition of proliferation or induction of apoptosis (Fig. 1e-f, Supplemental Fig. 4a). While iron prevented MO-OH-Nap-induced alterations in acetylated histone levels, the SAHA-treated cells were unaffected by the addition of iron (Supplemental Fig. 4b).

3.2. Iron prevents MO-OH-Nap mediated induction of the unfolded protein response

Our previous studies demonstrated that MO-OH-Nap induces upregulation of markers associated with the UPR in MM cells [15], however, whether iron chelators induce similar effects in MM cells has not yet been reported. We therefore evaluated the effects of DFO treatment on markers of the UPR and observed increases in protein levels of ATF4, CHOP, p-eIF2α and IRE1 in a concentration-dependent manner in MM cells (Fig. 2a). As shown by qRT-PCR, 24 h treatment with MO-OH-Nap promotes expression of UPR-associated genes, including ATF4, CHOP, and PERK and co-incubation with iron prevents this upregulation (Fig. 2b). The increase in p-eIF2α, ATF4, and CHOP protein levels induced by MO-OH-Nap and DFO can be prevented by co-incubation with iron (Fig. 2c and Supplemental Fig. 5). In addition, MO-OH-Nap induces XBP-1 splicing from its pro- to its active form by 24 h and this effect is blocked by the addition of AFS (Fig. 2d). Interestingly, both MO-OH-Nap and DFO induced cleavage of PERK, which was prevented by co-incubation with iron (Supplemental Fig. 6).

3.3. MO-OH-Nap chelates iron

To more directly address the hypothesis that MO-OH-Nap chelates iron, we conducted a ferrozine-based assay with MO-OH-Nap and DFO. In this cell-free assay, ferrozine produces a color change when it binds ferrous iron, which can be inhibited by the addition of a chelator. As shown in Fig. 3a, formation of the ferrozine-Fe complex was decreased by both MO-OH-Nap and DFO in a concentration-dependent manner. Under conditions where equal concentrations of ferrozine, DFO and MO-OH-Nap were used, DFO and MO-OH-Nap chelated 91% and 83% of iron, respectively.

3.4. MO-OH-Nap induces an upregulation of transferrin receptor

To address how MO-OH-Nap may affect intracellular iron homeostasis, we investigated MO-OH-Nap's effects on the expression of transferrin receptor 1 (TFR1). Under conditions of cellular iron deprivation TFR1 becomes upregulated in order to increase iron uptake [18]. Examination of TFR1 transcript levels via qRT-PCR show MO-OH-Nap and DFO upregulate TFR1 mRNA by 24 h and that this upregulation is reversed by the addition of AFS (Fig. 3b). Treatment with MO-OH-Nap or DFO induced an increase in TFR1 surface protein as measured by flow cytometry (Fig. 3c, Supplemental 7a) as well as an overall increase in TFR1 protein levels as assessed by western blot analysis (Supplemental Fig. 7b). The MO-OH-Nap-induced increase in TFR1 protein levels was also prevented by co-incubation with exogenous iron (Supplemental Fig. 7c).

3.5. MO-OH-Nap causes a cell-cycle arrest

Previous reports suggest that iron deprivation causes cells to accumulate in the G1 phase of the cell cycle, which likely is linked to iron's vital role in DNA synthesis [19]. Cell cycle analysis revealed an accumulation of MM cells in G0-G1 and a decrease of cells in S and G2-M phases when MO-OH-Nap was used alone but not when co-incubated with iron (Fig. 4). DFO promoted a similar effect as MO-OH-Nap, but to
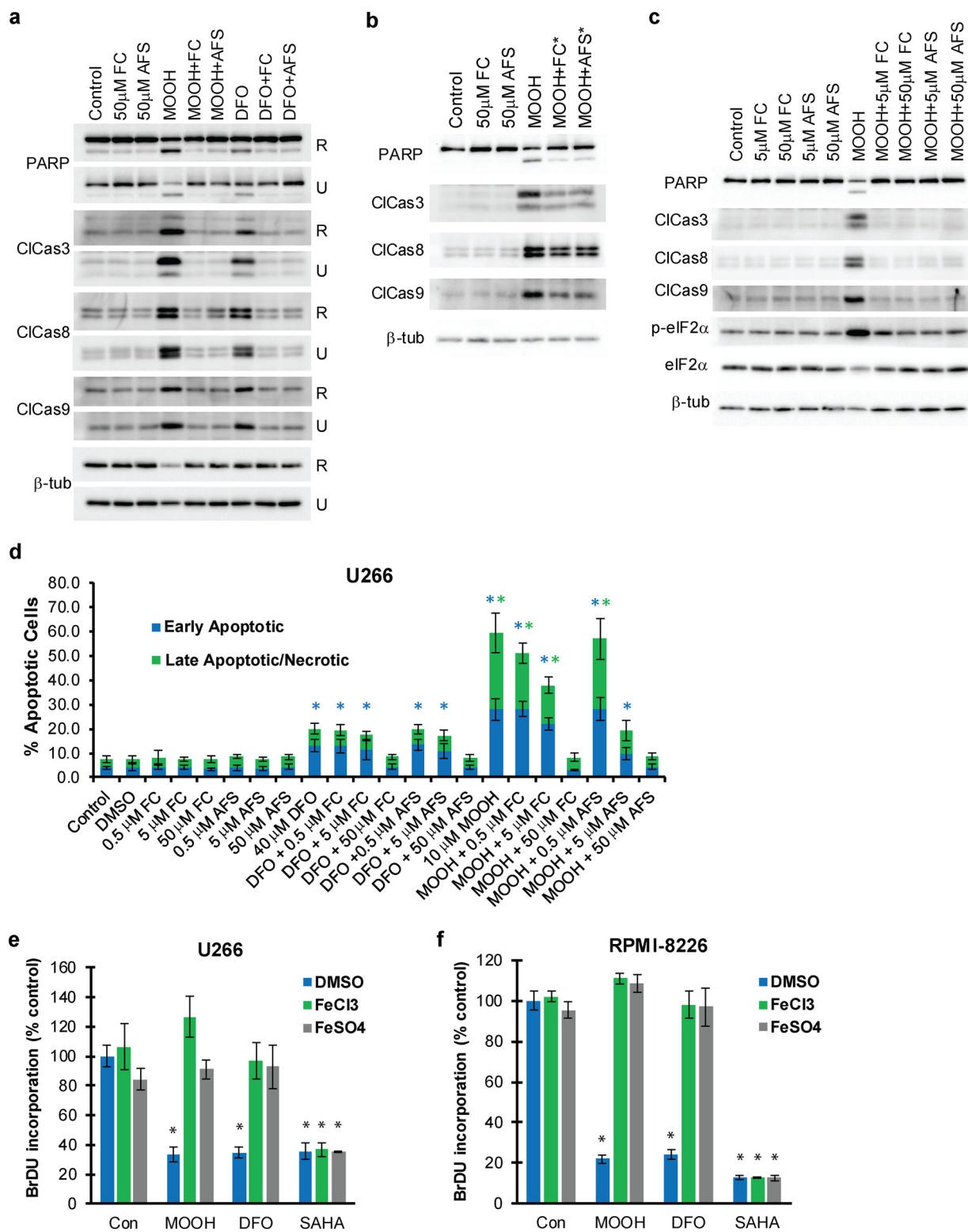
Fig. 1. Iron prevents the cytotoxic effects of MO-OH-Nap treatment in MM cells. a) U266 (U) and RPMI-8226 (R) cells were treated for 48 h with solvent control (DMSO), MO-OH-Nap (denoted as MOOH; 10 μM for U226 and 2.5 μM for RPMI), or 40 μM DFO in the presence or absence of 50 μM FC and 50μM AFS. Immunoblot analysis of cell lysates was performed using antibodies to detect PARP, cleaved caspases (3, 8, and 9) and β-tubulin (loading control). b) U266 cells were treated for 48 h with solvent control or 10 μM MO-OH-Nap. 50μM of AFS or FC were added 24 h after the addition of MO-OH-Nap. PARP, cleaved caspases (3, 8, and 9) and β-tubulin were detected by immunoblot. c) U266 cells were treated with DMSO or 10 μM MO-OH-Nap in the presence or absence of either 5 μM or 50 μM FC or AFS for 48 h. Protein levels of PARP, cleaved caspases (3, 8, and 9), p-eIF2α, eIF2α and β-tubulin were assessed by immunoblot. Immunoblots (a–c) are representative of three independent experiments. d) U226 cells were treated for 48 h with FC, AFS, MO-OH-Nap (10 μM), and DFO (40 μM). Percentage of early apoptotic and late apoptotic/necrotic cells were determined via flow cytometry. Early apoptotic cells are defined as AnnexinV + ,PI- while late apoptotic/necrotic cells are defined as AnnexinV + ,PI + . Data are shown as mean ± S.D. (n = 3) * denotes p < 0.05 for comparison to the vehicle-only control sample. e) BrdU incorporation was measured in U266 and RPMI-8226 cells treated with MO-OH-Nap (2.5 μM for RPMI-8226 and 10 μM for U266), 40 μM DFO, or 1 μM SAHA in the presence of solvent control (DMSO) or 50 μM AFS/FC. Data are shown as mean (normalized to control) ± S.D. (n = 3). *denoted p < 0.05 for comparison to the vehicle-only control.
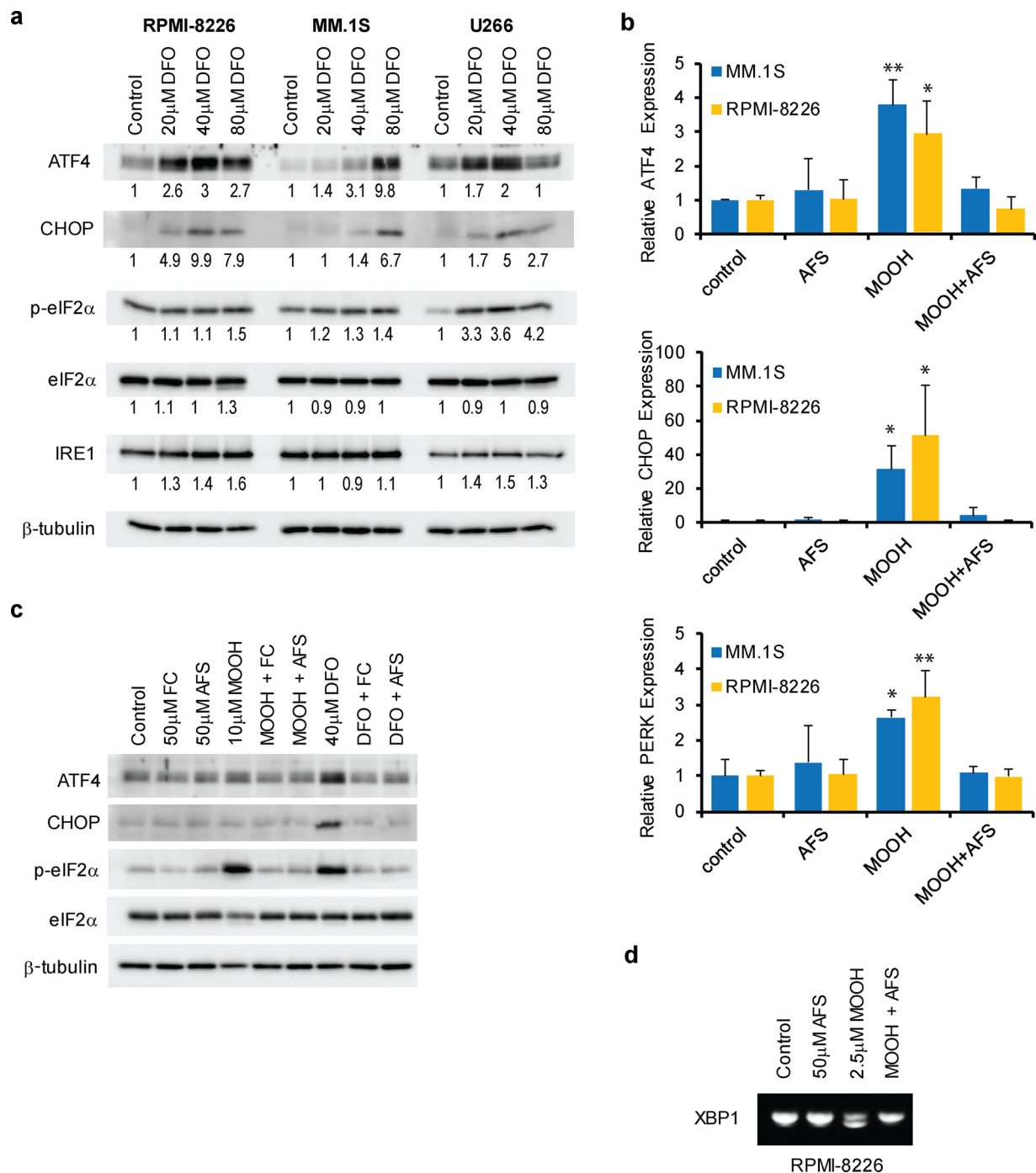
Fig. 2. Iron prevents MO-OH-Nap mediated induction of the unfolded protein response. a) U266, MM.1S, and RPMI-8226 cells were treated for 48 h with DMSO (solvent control) or various concentrations of DFO. Protein levels of ATF4, CHOP, p-eIF2α, eIF2α, IRE1 and β-tubulin (loading control) were measured by immunoblot. Densitometric analysis of the proteins of interest (normalized to loading control) for the treated cells normalized to untreated (control) cells is shown. Immunoblots are representative of three independent experiments. b) qRT-PCR analysis of ATF4, CHOP, and PERK mRNA levels in MM.1S and RPMI-8226 cell lines. Cells were exposed to DMSO, 2.5 μM MO-OH-Nap (MOOH) or 40 μM DFO in the presence or absence of 50 μM AFS for a period of 24 h. Data are shown as mean (normalized to control) ± S.D. (n = 3) ** denotes p < 0.01, *denotes p < 0.05 for comparison to the vehicle only control. c) U266 cells were treated for 48 h with DMSO, MO-OH-Nap or DFO in the presence or absence of FC and AFS. Protein levels of ATF4, CHOP, p-eIF2α, eIF2α and β-tubulin were measured by immunoblot. Immunoblots are representative of three independent experiments. d) PCR fragments showing XBP-1 slicing in PRMI-8226 cells following 24 h MO-OH-Nap and DFO treatment. Top band and bottom bands represent unspliced and spliced forms, respectively. This gel is representative of three independent experiments.

a lesser extent (Fig. 4).

3.6. MO-OH-Nap does not increase ROS

Because bound iron can participate in redox cycling we examined if MO-OH-Nap treatment promotes changes in intracellular reactive oxygen species (ROS) using the H2DCF-DA probe and flow cytometric analysis. At 24 and 48 h there were no changes in H2DCF-DA fluorescence levels in either MO-OH-Nap- or DFO-treated cells, suggesting neither compound promotes ROS generation in MM cells (Supplemental Fig. 8).
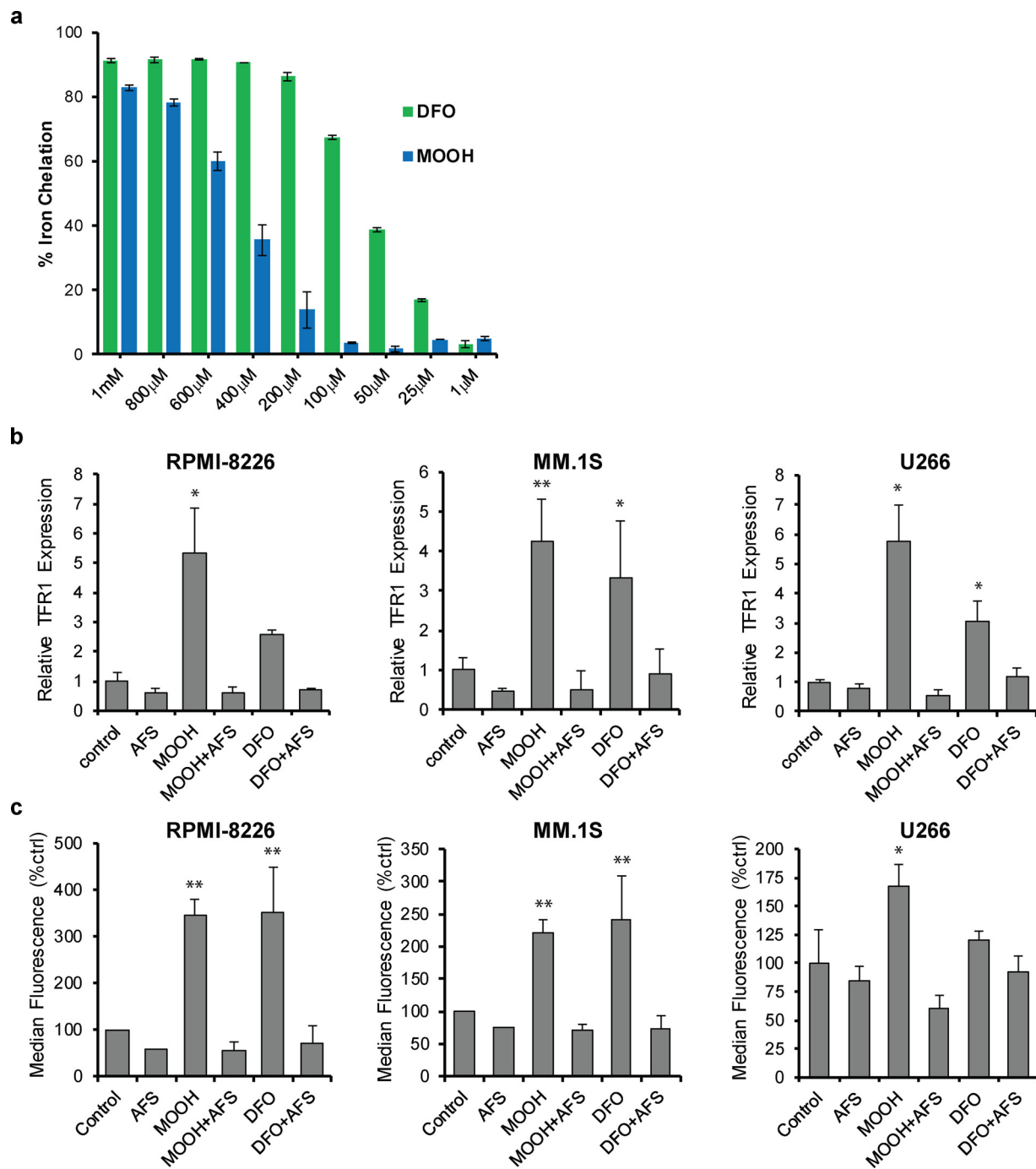
Fig. 3. MO-OH-Nap complexes iron and upregulates transferrin receptor (TFR1) expression in MM cells. a) Ferrozine assay showing relative amounts of iron chelation for various concentrations of MO-OH-Nap (MOOH) and DFO in the presence of AFS (0.25 mM) and Ferrozine (1 mM). Data was normalized to a control sample containing Ferrozine and AFS. Error bars denote S.D. b) qRT-PCR analysis of TFR1 transcript levels in MM.1S, RPMI-8226, and U266 cells treated for 24 h with MO-OH-Nap (MOOH; 2.5 μM for RPMI-8226/MM.1S and 10 μM for U266) or 40 μM DFO with or without 50 μM AFS. Data are normalized to expression values from the solvent only control. Error bars denote S.D., ** denotes $p < 0.01$, *denotes $p < 0.05$ for comparison to control. c) Flow cytometric analysis of TFR1 surface levels. Cells were treated for 48 h using the same concentration of drugs as in panel A. The bar graphs show median fluorescence values normalized to control (n = 3, error bars denote S.D., ** denotes $p < 0.01$, *denotes $p < 0.05$).

3.7. MO-OH-Nap, but not DFO, is synergistic with bortezomib

We previously reported that MO-OH-Nap and bortezomib induce synergistic cytotoxic effect in MM cells [15]. In contrast to the synergistic interaction observed between MO-OH-Nap and bortezomib, isobologram analysis of BrdU incorporation assays of DFO- and bortezomib-treated cells revealed an antagonistic interaction with combination indices (CI) greater than 1: RPMI-8226 CI for $IC_{30} = 1.98$; CI for $IC_{50} = 1.46$; U266: CI for $IC_{30} = 1.34$, CI for $IC_{50} = 1.41$ (Fig. 5).

3.8. MO-OH-Nap alters hepatosplenic macrophage iron consumption

To begin to evaluate the *in vivo* effects of MO-OH-Nap we performed dose escalation studies in CD-1 mice. No toxicities were observed at single doses up to 9.4 mg/kg IV, which represented the maximum dose that could be injected due to drug solubility issues. Multi-dose studies
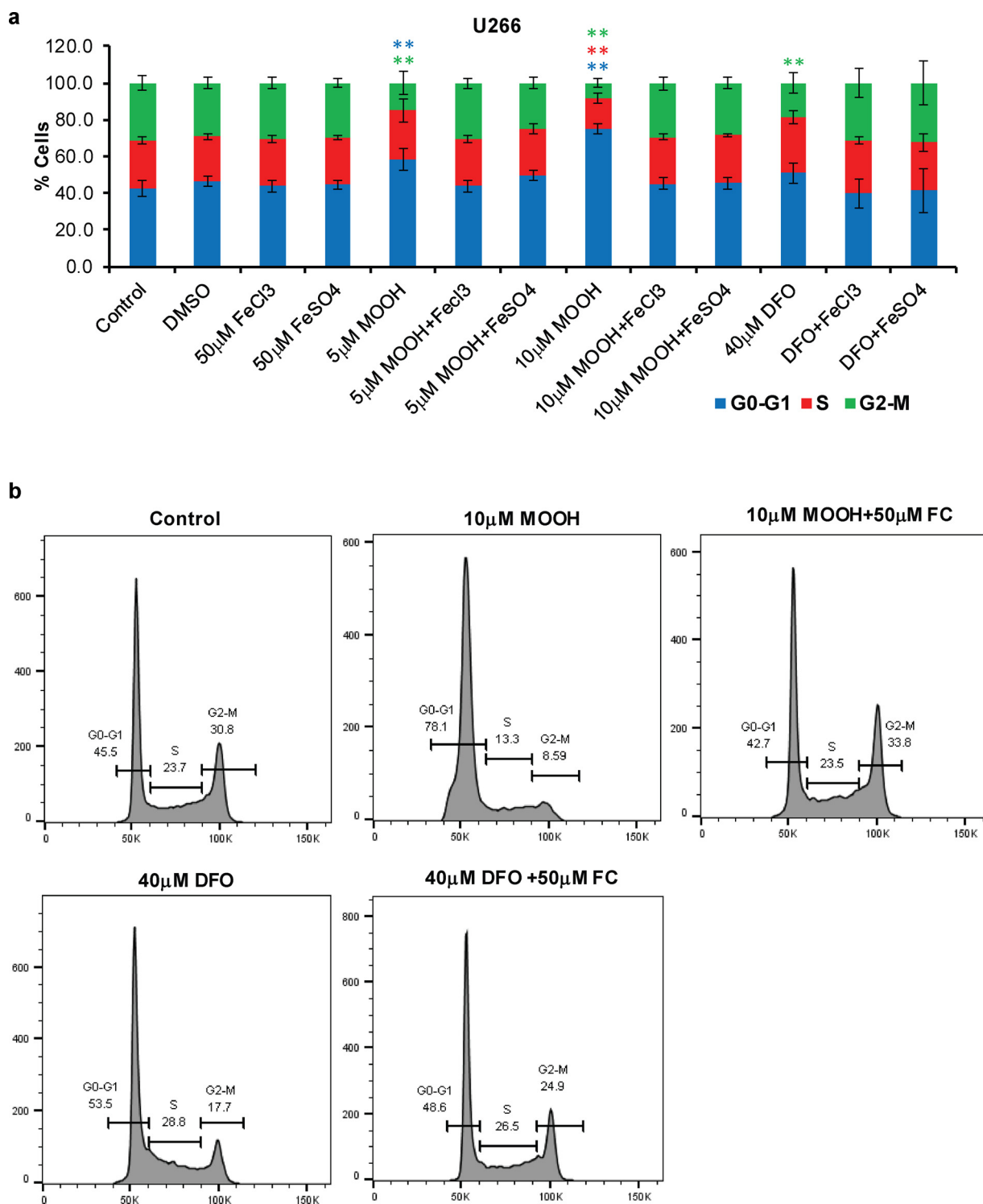
Fig. 4. MO-OH-Nap disrupts cell cycle progression. a) U266 cells were treated with DMSO, MO-OH-Nap (MOOH) or DFO with or without FC and AFS for 48 h. Cell cycle was measured via flow cytometry analysis. Data are shown as mean ± S.D. (n = 3) ** denotes p < 0.01, * denotes p < 0.05 for comparison to the vehicle only control. b) Representative flow histograms from data shown in panel a.

(9.4 mg/kg MO-OH-Nap 3 times per week for 4 weeks, n = 2) were then performed. Mice injected with MO-OH-Nap were grossly and histologically normal (Supplemental Fig. 9). No effects on hematological, renal, or hepatic function were observed (Supplemental Tables 2 and 3). Prussian blue staining of liver and spleen sections was performed to identify differences in iron levels between control and MO-OH-Nap-treated mice (Fig. 6). As would be expected, there was a lack of Prussian blue staining in the liver samples from control animals. Analysis of

sections from the livers of MO-OH-Nap-treated animals revealed stainable iron within Kupffer cells (1-2+) while adjacent bile ducts and hepatocytes were negative. As compared to controls, spleens from treated mice showed a marked increase in the number of red pulp macrophages containing iron, consistent with macrophage consumption of MO-OH-Nap-iron complexes. Finally, to assess the metabolic stability of MO-OH-Nap, studies were performed with mouse S9 fractions (liver homogenate isolated after centrifugation at 9000 g) to
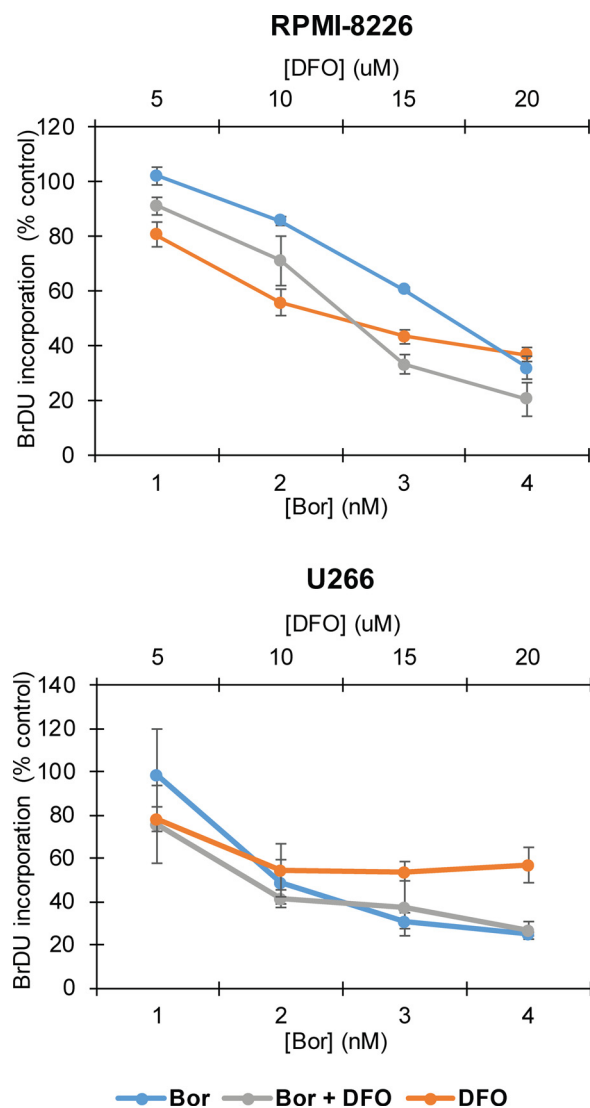
RPMI-8226

[DFO] (uM)

U266

[DFO] (uM)

Bor   **Bor + DFO**   **DFO**

Fig. 5. DFO is not synergistic with bortezomib. RPMI-8226 and U266 cells were treated with increasing concentrations bortezomib (Bor) and DFO. BrdU incorporation was measured after 48 h. Data are shown as mean ± S.D. (n = 3).

evaluate phase I and phase II metabolism. Minimal (< 15%) metabolism was observed in the presence of mouse S9 fraction, indicating that the compound is not undergoing cytochrome P450-mediated or phase II metabolism (Supplemental Fig. 10). Diclofenac, 7-HC, and testosterone were chosen as controls because they display known slow, medium, and fast metabolism, respectively. No additional peaks specific to predicted phase I or phase II metabolites were detected by LC/MS/MS following incubation of MO-OH-Nap in S9 fractions (data not shown).

4. Discussion

MM cells, by virtue of their high protein synthetic rate, are uniquely sensitive to therapeutic strategies which induce ER stress and the UPR. We had previously demonstrated that the novel α-substituted tropolone, MO-OH-Nap, induces apoptosis of MM cells in a UPR-dependent manner [15]. Due to this finding, we believe that tropolones are promising developmental candidates for MM therapy, and further studies on their anti-MM mechanisms of action are warranted. While previous studies suggested that related tropolones have activity as HDAC inhibitors [10], we found that MO-OH-Nap and the pan-HDAC inhibitor SAHA had unique gene expression profiles, consistent with disparate mechanisms of action [15]. Our current studies have focused on the

activity of MO-OH-Nap as an iron chelator to better define this agent's mechanism of action.

We compared MO-OH-Nap to the clinically approved iron chelator DFO and found that both compounds have the ability to induce the UPR and trigger apoptosis in MM cells and that these effects are fully abrogated by co-incubation with iron. Furthermore, much like DFO, MO-OH-Nap promotes upregulation of TFR1 in MM cells and it can directly complex iron. These data suggest that the activity of MO-OH-Nap is in part dependent on its ability to chelate iron and deplete intracellular iron stores. While various studies show that tropolones can complex iron [20], there is limited *in vivo* data for tropolones with respect to iron chelating activity. One study using tropolone derivatives found that while all four tested compounds were able to bind iron (III) hydroxide, they were not able to reduce iron loads in a mouse model of hemosiderosis [21]. Recent findings demonstrate that beta-thujaplicin facilitates the absorption of iron in the gut of DMT1-deficient rats and ferroportin-deficient mice, thus allowing it to restore the movement of iron into cells in the absence of iron transport proteins. [22] Our studies reveal that MO-OH-Nap is well-tolerated following repeat dosing in mice and we observed evidence of MO-OH-Nap-induced effects on hepatosplenic macrophage iron consumption.

Iron plays a pivotal role in a variety of normal cellular processes, including DNA synthesis and cell cycle progression. The rate-limiting step of DNA synthesis is accomplished via the iron-dependent ribonucleotide reductase, which explains why iron deprivation causes cells to accumulate at the G1/S border [23,24]. It has long been suggested that cancer cells demonstrate an increased requirement for intracellular iron and that pathways related to iron metabolism are deregulated. Some neoplastic cells express higher levels of iron import proteins, such as TFR1 and divalent metal transporter 1 (DMT1), while others can mediate iron uptake through non-receptor mediated pinocytosis [25–28]. A recent study found that MM cell lines have increased intracellular levels of iron as compared to normal cells, possibly due to decreased expression of the iron exporter ferroportin [29]. Several studies have suggested that iron chelators have anti-cancer activities [30]. There is increasing evidence for a complex interplay between the UPR and iron homeostasis, including the observations that ER stress can alter the expression profile of iron-related genes and that iron overload is associated with increased expression of ER chaperones [31–33]. On the other hand, exceedingly high levels of iron can be detrimental to cellular survival under certain conditions. Ferroptosis can occur when iron metabolism generates toxic reactive oxygen species that cause lipid peroxidation and cell death [34]. MM cell lines were shown to be less sensitive to an agent which induces ferroptotic cell death compared to diffuse large B cell lymphoma cell lines [35], demonstrating the complex relationship between iron and cell death pathways in MM.

Iron chelators have been shown to induce cytotoxic effects in MM cell lines. Kamihara et al., demonstrated that the clinically used iron chelator, deferasirox, induces caspase cleavage and apoptosis in MM cell lines [29]. Pullarkat et al., reported the cytotoxic activities of DFO and deferasirox in MM cells as being the result of autophagy-induced iron deprivation [36]. Likewise, di-2-pyridylketone 4,4-dimethyl-3-thiosemicarbazone (Dp44mT) is a novel cytotoxic agent that forms redox-active metal complexes to elevate ROS-production and can induce apoptosis in MM cells [37]. Interestingly, Dp44mT induces the upregulation of UPR-associated proteins including ATF4, CHOP, and p-eIF2α and promotes XBP-1 mRNA splicing in neuroepithelioma cell lines [38]. Such findings parallel our own results with MO-OH-Nap in MM cells. *In vivo* efficacy for Dp44mT in regards to MM has not been reported, however Dp44mT was shown to inhibit tumor growth in various other murine cancer models [39–41]. The solubility of MO-OH-Nap in biologically relevant solvents limited our ability to reach the maximally tolerated dose and perform *in vivo* efficacy studies in mouse MM models. However, studies are ongoing to develop analogues of MO-OH-Nap that will be tested *in vivo*.

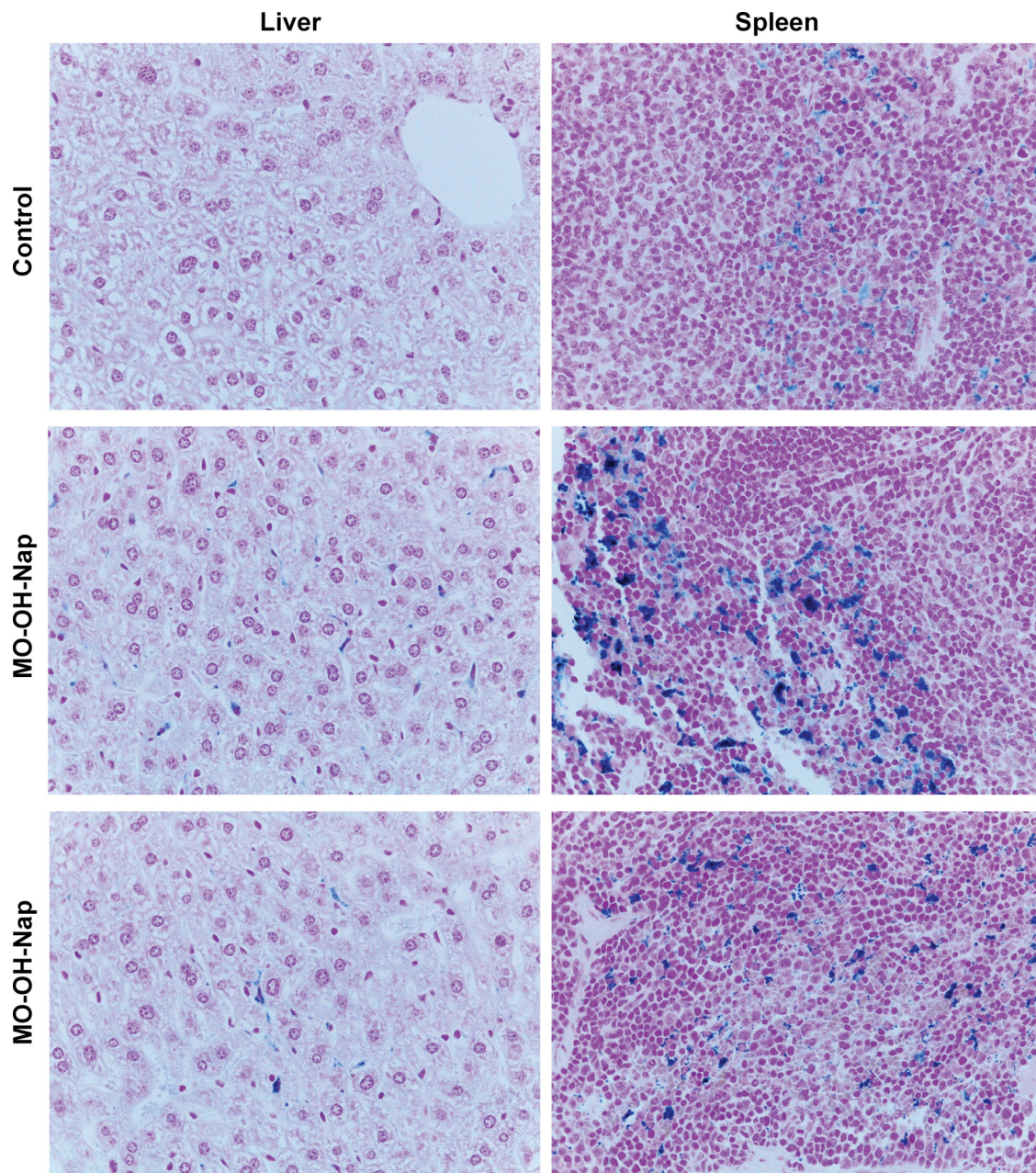Our previous findings show that MO-OH-Nap behaves

Liver **Spleen**

Fig. 6. MO-OH-Nap disrupts hepatosplenic iron handling. Prussian blue staining of liver and spleen sections (400x) from control and MO-OH-Nap (MOOH)-treated mice (9.4 mg/kg IV three times a week for four weeks). (For interpretation of the references to colour in this figure legend, the reader is referred to the web version of this article).

synergistically with the proteasome inhibitor bortezomib which is clinically relevant as proteasome inhibitors are widely used in the management of MM [15]. Here we demonstrate that DFO and bortezomib have an antagonistic affect when used in combination, indicating that MO-OH-Nap may have activity that is independent of its ability to bind iron. The results of previous microarray studies have suggested that tropolones have additional mechanisms of action, such as effects on DNA damage repair pathways [2,15], and the extent to which these effects are dependent on iron is as yet unknown. Furthermore, our findings indicate that MO-OH-Nap's effect on histone acetylation, while dependent on iron, is likely indirect. The mechanism by which MO-OH-Nap modulates histone modifications will require further investigation as the possibility remains that by binding iron MO-OH-Nap may disrupt the activity of an iron-dependent metalloenzyme.

In summary, our studies demonstrate that MO-OH-Nap's ability to

induce the UPR and apoptosis is iron-dependent. These findings are relevant as they not only provide insight into the mechanism of action of a novel tropolone, but also provide further rationale for investigating the therapeutic potential of iron-chelating agents to induce the UPR and apoptosis in MM. Future studies will focus on better understanding the molecular mechanisms of MO-OH-Nap and structure-function analysis of new generations of tropolone derivatives in order to evaluate these agents' potential as a novel anti-MM therapy.

5. Compliance with ethical standards

The authors declare that they have no conflict of interest.

All applicable international, national, and/or institutional guidelines for the care and use of animals were followed. All procedures performed in studies involving animals were in accordance with the

ethical standards of the institution or practice at which the studies were conducted.

This article does not contain any studies with human participants performed by any of the authors.

Acknowledgments

References

[1] C.J. Hsiao, S.H. Hsiao, W.L. Chen, J.H. Guh, G. Hsiao, Y.J. Chan, T.H. Lee, C.L. Chung, Pycnidione, a fungus-derived agent, induces cell cycle arrest and apoptosis in A549 human lung cancer cells, Chem. Biol. Interact. 197 (2012) 23–30, https://doi.org/10.1016/j.cbi.2012.03.004.

[2] J. Li, E.R. Falcone, S.A. Holstein, A.C. Anderson, D.L. Wright, A.J. Wiemer, Novel alpha-substituted tropolones promote potent and selective caspase-dependent leukemia cell apoptosis, Pharmacol. Res. 113 (2016) 438–448, https://doi.org/10.1016/j.phrs.2016.09.020.

[3] S.N. Ononye, M.D. Vanheyst, C. Giardina, D.L. Wright, A.C. Anderson, Studies on the antiproliferative effects of tropolone derivatives in Jurkat T-lymphocyte cells, Bioorg. Med. Chem. 22 (2014) 2188–2193, https://doi.org/10.1016/j.bmc.2014.02.018.

[4] S. Liu, H. Yamauchi, Hinokitiol, a metal chelator derived from natural plants, suppresses cell growth and disrupts androgen receptor signaling in prostate carcinoma cell lines, Biochem. Biophys. Res. Commun. 351 (2006) 26–32, https://doi.org/10.1016/j.bbrc.2006.09.166.

[5] C.H. Huang, T. Jayakumar, C.C. Chang, T.H. Fong, S.H. Lu, P.A. Thomas, C.S. Choy, J.R. Sheu, Hinokitiol exerts anticancer activity through downregulation of MMPs 9/2 and enhancement of catalase and SOD Enzymes: in vivo augmentation of lung histoarchitecture, Molecules 20 (2015) 17720–17734, https://doi.org/10.3390/molecules201017720.

[6] C.H. Huang, S.H. Lu, C.C. Chang, P.A. Thomas, T. Jayakumar, J.R. Sheu, Hinokitiol, a tropolone derivative, inhibits mouse melanoma (B16-F10) cell migration and in vivo tumor formation, Eur. J. Pharmacol. 746 (2015) 148–157, https://doi.org/10.1016/j.ejphar.2014.11.011.

[7] S.M. Chen, B.Y. Wang, C.H. Lee, H.T. Lee, J.J. Li, G.C. Hong, Y.C. Hung, P.J. Chien, C.Y. Chang, L.S. Hsu, W.W. Chang, Hinokitiol up-regulates miR-494-3p to suppress BMI1 expression and inhibits self-renewal of breast cancer stem/progenitor cells, Oncotarget 8 (2017) 76057–76068, https://doi.org/10.18632/oncotarget.18648.

[8] K. Nakano, T. Chigira, T. Miyafusa, S. Nagatoishi, J.M. Caaveiro, K. Tsumoto, Discovery and characterization of natural tropolones as inhibitors of the antibacterial target CapF from Staphylococcus aureus, Sci. Rep. 5 (2015) 15337, https://doi.org/10.1038/srep15337.

[9] J.L. Fullagar, A.L. Garner, A.K. Struss, J.A. Day, D.P. Martin, J. Yu, X. Cai, K.D. Janda, S.M. Cohen, Antagonism of a zinc metalloprotease using a unique metal-chelating scaffold: tropolones as inhibitors of P. aeruginosa elastase, Chem. Commun. (Camb.) 49 (2013) 3197–3199, https://doi.org/10.1039/c3cc41191e.

[10] S.N. Ononye, M.D. VanHeyst, E.Z. Oblak, W. Zhou, M. Ammar, A.C. Anderson, D.L. Wright, Tropolones as lead-like natural products: the development of potent and selective histone deacetylase inhibitors, ACS Med. Chem. Lett. 4 (2013) 757–761, https://doi.org/10.1021/ml400158k.

[11] F.W. Bryant, BE, Formation constants of metal complexes of tropolone and its derivatives II, J. Am. Chem. Soc. 76 (1954) 1696–1697.

[12] O. Menis, B.E. McClellan, D.S. Bright, Determination of the formation constants of iron(III) and vanadium(V) with β-isopropyltropolone using the extraction method, Anal. Chem. 43 (1971) 431–435.

[13] M.S. Oka, Mutual determination of iron(III) and tropolone, and the formation constant of their complex, Bunseki Kagaku 7 (1958) 215–219.

[14] A.M. Noone, N. Howlander, M. Krapcho, D. Miller, A. Brest, M. Yu, J. Ruhl, Z. Tatalovich, A. Mariotto, D.R. Lewis, H.S. Chen, E.J. Feuer, K.A. Cronin, SEER Cancer Statistics Review, (2018), pp. 1975–2015 https://seer.cancer.gov/csr/1975_2015/.

[15] S.L. Haney, C. Allen, M.L. Varney, K.M. Dykstra, E.R. Falcone, S.H. Colligan, Q. Hu, A.M. Aldridge, D.L. Wright, A.J. Wiemer, S.A. Holstein, Novel tropolones induce the

[16] D. Wlodkowic, J. Skommer, Z. Darzynkiewicz, Flow cytometry-based apoptosis detection, Methods Mol. Biol. 559 (2009) 19–32, https://doi.org/10.1007/978-1-60327-017-5_2.

[17] T.C. Chou, P. Talalay, Quantitative analysis of dose-effect relationships: the combined effects of multiple drugs or enzyme inhibitors, Adv. Enzyme Regul. 22 (1984) 27–55.

[18] Y. Yu, Z. Kovacevic, D.R. Richardson, Tuning cell cycle regulation with an iron key, Cell Cycle 6 (2007) 1982–1994, https://doi.org/10.4161/cc.6.16.4603.

[19] C. Brodie, G. Siriwardana, J. Lucas, R. Schleicher, N. Terada, A. Szepesi, E. Gelfand, P. Seligman, Neuroblastoma sensitivity to growth inhibition by deferrioxamine: evidence for a block in G1 phase of the cell cycle, Cancer Res. 53 (1993) 3968–3975.

[20] K. Murakami, Y. Ohara, M. Haneda, R. Tsubouchi, M. Yoshino, Prooxidant action of hinokitiol: hinokitiol-iron dependent generation of reactive oxygen species, Basic Clin. Pharmacol. Toxicol. 97 (2005) 392–394, https://doi.org/10.1111/j.1742-7843.2005.pto_214.x.

[21] C.G. Pitt, G. Gupta, W.E. Estes, H. Rosenkrantz, J.J. Metterville, A.L. Crumbliss, R.A. Palmer, K.W. Nordquest, K.A. Hardy, D.R. Whitcomb, B.R. Byers, J.E. Arceneaux, C.G. Gaines, C.V. Sciortino, The selection and evaluation of new chelating agents for the treatment of iron overload, J. Pharmacol. Exp. Ther. 208 (1979) 12–18.

[22] A.S. Grillo, A.M. SantaMaria, M.D. Kafina, A.G. Cioffi, N.C. Huston, M. Han, Y.A. Seo, Y.Y. Yien, C. Nardone, A.V. Menon, J. Fan, D.C. Svoboda, J.B. Anderson, J.D. Hong, B.G. Nicolau, K. Subedi, A.A. Gewirth, M. Wessling-Resnick, J. Kim, B.H. Paw, M.D. Burke, Restored iron transport by a small molecule promotes absorption and hemoglobinization in animals, Science 356 (2017) 608–616, https://doi.org/10.1126/science.aah3862.

[23] N. Terada, R. Or, A. Szepesi, J.J. Lucas, E.W. Gelfand, Definition of the roles for iron and essential fatty acids in cell cycle progression of normal human T lymphocytes, Exp. Cell Res. 204 (1993) 260–267, https://doi.org/10.1006/excr.1993.1032.

[24] L. Thelander, A. Graslund, Mechanism of inhibition of mammalian ribonucleotide reductase by the iron chelate of 1-formylisoquinoline thiosemicarbazone. Destruction of the tyrosine free radical of the enzyme in an oxygen-requiring reaction, J. Biol. Chem. 258 (1983) 4063–4066.

[25] K.C. Gatter, G. Brown, I.S. Trowbridge, R.E. Woolston, D.Y. Mason, Transferrin receptors in human tissues: their distribution and possible clinical relevance, J. Clin. Pathol. 36 (1983) 539–545.

[26] M.J. Brookes, S. Hughes, F.E. Turner, G. Reynolds, N. Sharma, T. Ismail, G. Berx, A.T. McKie, N. Hotchin, G.J. Anderson, T. Iqbal, C. Tselepis, Modulation of iron transport proteins in human colorectal carcinogenesis, Gut 55 (2006) 1449–1460, https://doi.org/10.1136/gut.2006.094060.

[27] D. Trinder, O. Zak, P. Aisen, Transferrin receptor-independent uptake of differic transferrin by human hepatoma cells with antisense inhibition of receptor expression, Hepatology 23 (1996) 1512–1520, https://doi.org/10.1053/jhep.1996.v23.pm0008675172.

[28] D.R. Richardson, E. Baker, The uptake of iron and transferrin by the human malignant melanoma cell, Biochim. Biophys. Acta 1053 (1990) 1–12.

[29] Y. Kamihara, K. Takada, T. Sato, Y. Kawano, K. Murase, Y. Arihara, S. Kikuchi, N. Hayasaka, M. Usami, S. Iyama, K. Miyanishi, Y. Sato, M. Kobune, J. Kato, The iron chelator deferasirox induces apoptosis by targeting oncogenic Pyk2/beta-catenin signaling in human multiple myeloma, Oncotarget 7 (2016) 64330–64341, https://doi.org/10.18632/oncotarget.11830.

[30] M.R. Bedford, S.J. Ford, R.D. Horniblow, T.H. Iqbal, C. Tselepis, Iron chelation in the treatment of cancer: a new role for deferasirox? J. Clin. Pharmacol. 53 (2013) 885–891, https://doi.org/10.1002/jcph.113.

[31] K.R. You, M.J. Liu, X.J. Han, Z.W. Lee, D.G. Kim, Transcriptional regulation of the human transferrin gene by GADD153 in hepatoma cells, Hepatology 38 (2003) 745–755, https://doi.org/10.1053/jhep.2003.50367.

[32] S.J. Oliveira, J.P. Pinto, G. Picarote, V.M. Costa, F. Carvalho, M. Rangel, M. de Sousa, S.F. de Almeida, ER stress-inducible factor CHOP affects the expression of hepcidin by modulating C/EBPalpha activity, PLoS One 4 (2009) e6618, https://doi.org/10.1371/journal.pone.0006618.

[33] C. Vecchi, G. Montosi, K. Zhang, I. Lamberti, S.A. Duncan, R.J. Kaufman, A. Pietrangelo, ER stress controls iron metabolism through induction of hepcidin, Science 325 (2009) 877–880, https://doi.org/10.1126/science.1176639.

[34] F. Thevenod, Iron and Its Role in Cancer Defense: A Double-Edged Sword, Met. Ions Life Sci. 18 (2018), https://doi.org/10.1515/9783110470734-021.

[35] W.S. Yang, R. SriRamaratnam, M.E. Welsch, K. Shimada, R. Skouta, V.S. Viswanathan, J.H. Cheah, P.A. Clemons, A.F. Shamji, C.B. Clish, L.M. Brown, A.W. Girotti, V.W. Cornish, S.L. Schreiber, B.R. Stockwell, Regulation of ferroptotic cancer cell death by GPX4, Cell 156 (2014) 317–331, https://doi.org/10.1016/j.cell.2013.12.010.

[36] V. Pullarkat, Z. Meng, C. Donohue, V.N. Yamamoto, S. Tomassetti, R. Bhatia, A. Krishnan, S.J. Forman, T.W. Synold, Iron chelators induce autophagic cell death in multiple myeloma cells, Leuk. Res. 38 (2014) 988–996, https://doi.org/10.1016/j.leukres.2014.06.005.

[37] E. Noulsri, D.R. Richardson, S. Lerdwana, S. Fucharoen, T. Yamagishi, D.S. Kalinowski, K. Pattanapanyasat, Antitumor activity and mechanism of action of the iron chelator, Dp44mT, against leukemic cells, Am. J. Hematol. 84 (2009) 170–176, https://doi.org/10.1002/ajh.21350.

[38] A.M. Merlot, N.H. Shafie, Y. Yu, V. Richardson, P.J. Jansson, S. Sahni, D.J. Lane, Z. Kovacevic, D.S. Kalinowski, D.R. Richardson, Mechanism of the induction of endoplasmic reticulum stress by the anti-cancer agent, di-2-pyridylketone 4,4-dimethyl-3-thiosemicarbazone (Dp44mT): activation of PERK/eIF2alpha, IRE1alpha,

ATF6 and calmodulin kinase, Biochem. Pharmacol. 109 (2016) 27–47, https://doi.org/10.1016/j.bcp.2016.04.001.

[39] J. Yuan, D.B. Lovejoy, D.R. Richardson, Novel di-2-pyridyl-derived iron chelators with marked and selective antitumor activity: in vitro and in vivo assessment, Blood 104 (2004) 1450–1458, https://doi.org/10.1182/blood-2004-03-0868.

[40] Z.L. Guo, D.R. Richardson, D.S. Kalinowski, Z. Kovacevic, K.C. Tan-Un, G.C. Chan, The novel thiosemicarbazone, di-2-pyridylketone 4-cyclohexyl-4-methyl-3-thiosemicarbazone (DpC), inhibits neuroblastoma growth in vitro and in vivo via multiple mechanisms, J. Hematol. Oncol. 9 (2016) 98, https://doi.org/10.1186/s13045-016-0330-x.

[41] P. Li, X. Zheng, K. Shou, Y. Niu, C. Jian, Y. Zhao, W. Yi, X. Hu, A. Yu, The iron chelator Dp44mT suppresses osteosarcoma's proliferation, invasion and migration: in vitro and in vivo, Am. J. Transl. Res. 8 (2016) 5370–5385.